




# Simple Label-Free DNA Sensor Based on CeO<sub>2</sub> Nanorods Decorated with Ppy Nanoparticles

NGUYEN THI NGUYET,<sup>1,3</sup> VU VAN THU,<sup>4</sup> HOANG LAN,<sup>1</sup> TRAN TRUNG,<sup>3</sup>  
ANH-TUAN LE,<sup>2,5</sup> VUONG-HUNG PHAM,<sup>1,6</sup>  
and PHUONG DINH TAM <sup>1,2,5,7,8</sup>

1.—Advanced Institute for Science and Technology, Hanoi University of Science and Technology, No. 1 DaiCoViet Road, Hanoi 12116, Vietnam. 2.—Faculty of Material Science and Engineering, Phenikaa University, Yen Nghia, Ha-Dong District, Hanoi 12116, Vietnam. 3.—Hung Yen University of Technology and Education, Hung Yen 17000, Vietnam. 4.—Faculty of Occupational Safety and Health, Trade Union University, Hanoi 12116, Vietnam. 5.—Phenikaa University Nano Institute, Phenikaa University, Hanoi 12116, Vietnam. 6.—e-mail: [vuong.phamhung@hust.edu.vn](mailto:vuong.phamhung@hust.edu.vn). 7.—e-mail: [tam.phuongdinh@phenikaa-uni.edu.vn](mailto:tam.phuongdinh@phenikaa-uni.edu.vn). 8.—e-mail: [phuongdinhnam@gmail.com](mailto:phuongdinhnam@gmail.com)

A facile label-free DNA sensor based on cerium oxide nanorods decorated with polypyrrole nanoparticles (CeO<sub>2</sub>-NRs/Ppy-NPs) matrix has been developed for detection of *Salmonella*. The sensor was fabricated by hydrothermal synthesis of CeO<sub>2</sub>-NRs on the microelectrode surface followed by *in situ* chemical oxidative polymerization of pyrrole on the CeO<sub>2</sub>-NRs to prepare a CeO<sub>2</sub>-NR/Ppy-NPs electrode. Single-stranded DNA (ssDNA) sequences were immobilized onto the modified microelectrode by covalent attachment. The properties of the material were explored by field-emission scanning electron microscopy, x-ray diffraction analysis, and Fourier-transform infrared spectroscopy techniques. The response of the DNA biosensor was investigated by electrochemical impedance spectroscopy with [Fe(CN)<sub>6</sub>]<sup>3-/4-</sup> as redox probe. The results showed that the response of the DNA biosensor exhibited good linearity within the range of  $1.0 \times 10^{-9}$  mol L<sup>-1</sup> to  $1.0 \times 10^{-6}$  mol L<sup>-1</sup> with sensitivity of  $14.7 \times 10^6$  Ω/mol L<sup>-1</sup> cm<sup>-1</sup>. The limit of detection and limit of quantification of the DNA biosensor were low, with values of  $2.86 \cdot 10^{-7}$  mol L<sup>-1</sup> and  $9.56 \cdot 10^{-7}$  mol L<sup>-1</sup>, respectively.

**Key words:** Nanocomposite, conducting polymer, biosensor, nanorod, CeO<sub>2</sub>

## INTRODUCTION

DNA sequence detection is very important for medical diagnostics, viral pathogen detection, and genomic identification. Conventional detection techniques include polymerase chain reaction (PCR),<sup>1</sup> real-time fluorescence PCR,<sup>2</sup> and enzyme-linked immunosorbent assay (ELISA).<sup>3</sup> However, these methods are very time consuming, expensive, and difficult to use on site for early detection. Thus, a

simple, effective detection approach must be developed for fast DNA detection.

An increasing number of DNA biosensors have been developed for DNA detection and reported in numerous scientific publications.<sup>4-6</sup> DNA hybridization detection depends on binding of various labels to biomolecules, including fluorescent dyes,<sup>7</sup> nanoparticles,<sup>8,9</sup> and redox-active enzymes.<sup>10,11</sup> However, these high-performance techniques are time consuming, expensive, and require labeling processes. The conformation of the DNA strand may also be modified, decreasing the precision of such DNA detection approaches. Label-free DNA detection techniques have thus been widely investigated.<sup>12</sup> These techniques measure changes in the

charge on the surface of an electrode due to the interaction with DNA probes. The detection limit of such DNA sensors is on the order of picomoles,<sup>13</sup> which is suitable for detection of DNA sequences at low concentration.

The use of nanostructured composite materials as supports for DNA immobilization has attracted increasing attention.<sup>14–16</sup> Among such nanostructured materials, cerium oxide (CeO<sub>2</sub>) has been widely studied due to its interesting properties, including biocompatibility, high isoelectric point (9.2), wide bandgap (3.4 eV), nontoxicity, electronic conductivity, and high electrochemical stability. Recently, CeO<sub>2</sub>-based DNA sensors were reported by several research groups. Gao et al.<sup>17</sup> investigated the use of a CeO<sub>2</sub> material-based DNA sensor to detect hydrogen peroxide in living cells through competitive coordination; their results showed that the fluorescence intensity is linearly correlated with the H<sub>2</sub>O<sub>2</sub> concentration in the range of 1 μM to 100 μM with a detection limit of 0.64 μM. A highly sensitive CeO<sub>2</sub>-NR-based DNA sensor was studied by our group.<sup>18</sup> In the work presented herein, the hydrothermal approach was used to synthesize CeO<sub>2</sub>-NRs. ssDNA sequences were immobilized onto the CeO<sub>2</sub>-NR-modified electrode by covalent attachment. The response of the DNA sensor was analyzed by electrochemical impedance spectroscopy using [Fe(CN)<sub>6</sub>]<sup>3-/4-</sup> as a redox probe. A linear response of the DNA sensor was found within the range of 0.01 μM to 2 μM. The detection limit of the DNA sensor was 0.01 μM, and its sensitivity was 3362.1 Ω μM<sup>-1</sup> cm<sup>-2</sup>.

Various studies have been performed on CeO<sub>2</sub> nanocomposites for biosensor applications. Rayapan and coworker<sup>19</sup> synthesized CeO<sub>2</sub>/polyaniline (PANI) nanocomposites using a hydroxide method for application in electrochemical biosensors to detect histamine. The prepared nanocomposites are biocompatible and possess catalytic properties and rapid electron transfer kinetics, which enhance the direct electron transfer between the enzyme and electrode. The biosensor had sensitivity of 724.94 μA cm<sup>-2</sup> mM<sup>-1</sup> with a linear range of 0.45 mM to 1.05 mM. In another study, an electrochemical biosensor with ceria–polyaniline core–shell structure was developed for detection of carbonic acid in blood. The sensor had sensitivity of 696.49 μA cm<sup>-2</sup> mM<sup>-1</sup> with a linear range of 1.32 mM to 2.32 mM.<sup>20</sup> Wang et al.<sup>21</sup> conducted one-step electrodeposition of hollow CeO<sub>2</sub>-ZrO<sub>2</sub> nanospheres and chitosan to fabricate a sensor for detection of DNA hybridization within a wide dynamic range of 1.63 × 10<sup>-13</sup> M to 1.63 × 10<sup>-8</sup> M and low detection limit of 1.0 × 10<sup>-13</sup> M. Zhang et al.<sup>22</sup> synthesized a CeO<sub>2</sub> nanoshuttle–carbon nanotube composite as a platform for impedance DNA hybridization sensing. The obtained material matrix could greatly enhance the loading of ssDNA probes, and improved the sensitivity of detecting target DNA. Qian et al.<sup>23</sup> developed a DNA sensor based on immobilization of DNA probes on the

surface of a CeO<sub>2</sub>/chitosan-modified electrode by metal coordination. The DNA biosensor exhibited high sensitivity and selectivity, wide dynamic range, satisfactory reproducibility, and stability. The fabricated biosensor could be utilized as a potential sensing platform for effective and convenient detection of foodborne pathogens.

In this work, we investigated a label-free DNA sensor based on CeO<sub>2</sub>-NRs decorated with Ppy-NPs for detection of *Salmonella*. The DNA sensor was characterized by electrochemical impedance spectroscopy (EIS). The introduction of Ppy-NPs increased the conductivity as well as the stability of the electrode, which shows potential for application as a DNA sensor for detection of biomolecules. A schematic of the DNA sensor fabrication is presented in Scheme 1.

## EXPERIMENTAL PROCEDURES

### Chemical Reagents

Cerium(III) nitrate hexahydrate [CeO(NO<sub>3</sub>)<sub>3</sub>•6H<sub>2</sub>O], dipotassium phosphate (K<sub>2</sub>HPO<sub>4</sub>), potassium dihydrogen phosphate (KH<sub>2</sub>PO<sub>4</sub>), hydrochloric acid (HCl), bovine serum albumin (BSA), 3-aminopropyltriethoxysilane (APTES), 1-ethyl-3-(dimethylaminopropyl) carbodiimide (EDC), 1-methylimidazole (MIA), and pyrrole were purchased from Sigma–Aldrich. Potassium hexacyanoferrate(III) (K<sub>3</sub>[Fe(CN)<sub>6</sub>]) and potassium hexacyanoferrate(II) (K<sub>4</sub>[Fe(CN)<sub>6</sub>]) were obtained from Beijing Chemical Reagents (China). All solutions were prepared using ultrapure water (18.2 MΩ·cm).

DNA immobilization buffer (I-buffer) was prepared with 10 mM Tris–HCl + 1 mM ethylenediaminetetraacetic acid (EDTA) + 0.1 M NaCl (pH 7). Hybridization buffer (H-buffer) comprised 10 mM phosphate-buffered saline (PBS) + 0.25 M NaCl (pH 7). Washing buffer (W-buffer) consisted of 10 mM Tris–HCl (pH 7). DNA hybridization detection buffer (E-buffer) contained 10 mM PBS + 10 mM NaCl (pH 7). The synthetic DNA sequences were as follows:

Probe DNA: 5'-GGCTGGTACCACCTCTTCTAC-CATGG-3'

Target DNA: 3'-CCGACCATGGTGGAGAA-GATGGTACC-5'

One-base-mismatched DNA: 3'-CCTACCATGG-TAGAGAAGGTGGTACC-5'

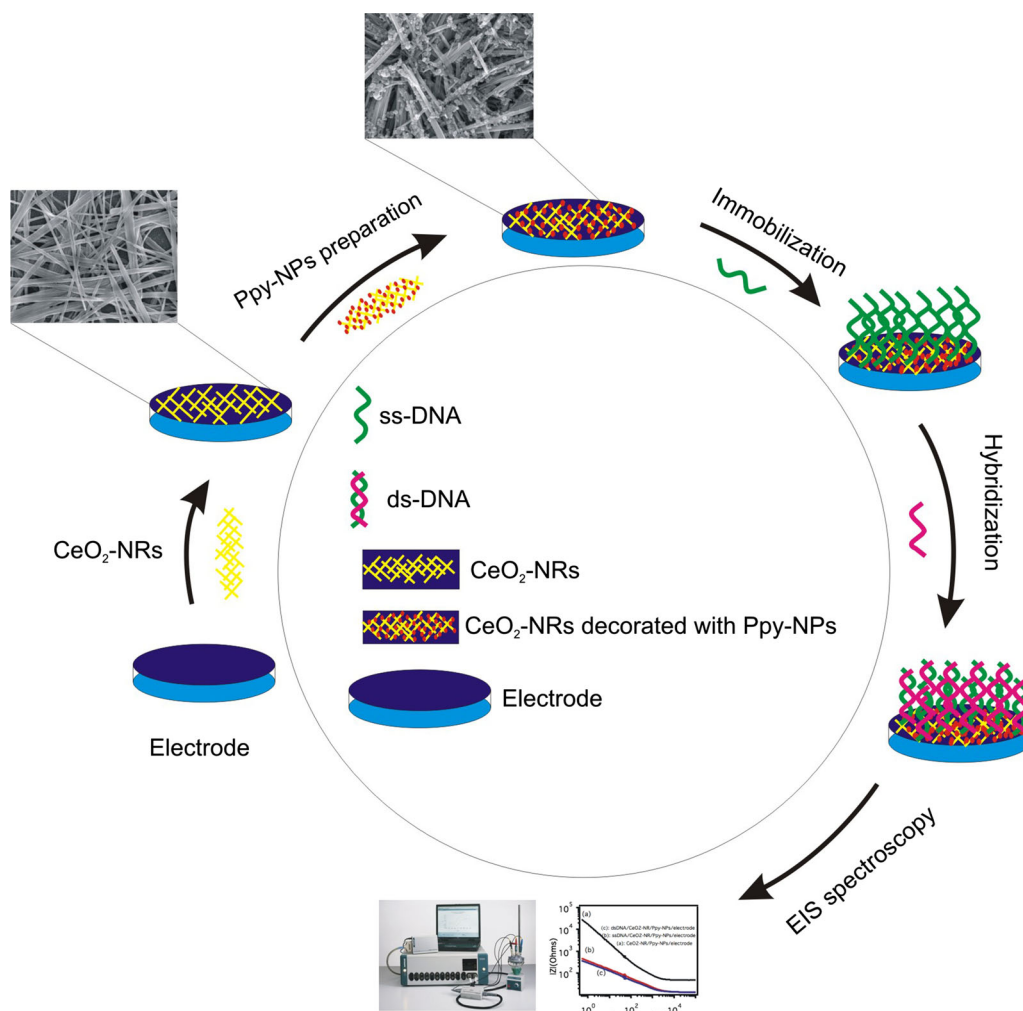
Two-base-mismatched DNA: 3'-CCTACCATGG-TAGAGAAGGTGGTACC-5'

Three-base-mismatched DNA: 3'-CCTACCATGG-TAGAGAAGGTGGTACC-5'

Noncomplementary (control sample): 5'-GGCTGGTACCACCTCTTCTACCATGG-3'

### CeO<sub>2</sub>-NR Synthesis

CeO<sub>2</sub>-NRs were prepared by a simple hydrothermal method. Ce(NO<sub>3</sub>)<sub>3</sub>•6H<sub>2</sub>O was dissolved in a solution



Scheme 1. Schematic of DNA sensor fabrication process.

including 30 ml HCl (1%), 10 ml KH<sub>2</sub>PO<sub>4</sub>:K<sub>2</sub>HPO<sub>4</sub>, and 30 ml distilled water. The sample was stirred for 30 min, and transferred into a 100-ml Teflon-lined stainless-steel autoclave, which was placed into a furnace. The temperature was changed to react at 150°C for 10 h followed by natural cooling to room temperature. The CeO<sub>2</sub>-NRs were washed with deionized water and dried in a vacuum oven for 6 h at 60°C.

### Preparation of CeO<sub>2</sub>-NRs Decorated with Ppy-NPs

The material was synthesized by *in situ* chemical oxidative polymerization of pyrrole on CeO<sub>2</sub> NRs in the presence of FeCl<sub>3</sub>·6H<sub>2</sub>O as an oxidant. A certain amount of CeO<sub>2</sub> NRs was added to FeCl<sub>3</sub>·6H<sub>2</sub>O (50 mg) solution under magnetic stirring for 30 min. The pyrrole monomer was injected slowly into the solution. Polymerization was carried out for 12 h under constant stirring. The obtained nanomaterial

was filtered, washed with ethanol and distilled water to remove any impurity, and dried at room temperature.

### Immobilization of ssDNA Probe

ssDNA probe immobilization was performed as follows: The electrode modified with CeO<sub>2</sub>-NRs decorated with Ppy-NP was immersed in APTES ethanol mixture for 1 h. The ssDNA strands were activated by EDC and stabilized by adding MIA. The EDC/MIA-activated ssDNA sequences were attached to the electrode surface via covalent bonding between the amine-group-modified CeO<sub>2</sub>-NRs decorated with Ppy-NPs and the phosphate group of the ssDNA sequence. The ssDNA/Ppy-NPs/CeO<sub>2</sub>-NRs electrode was incubated in deionized (DI) water at 37°C for 10 h. The electrode was immersed in BSA solution at room temperature for 30 min, rinsed with DI water, and dried in nitrogen flow to block nonspecific sites.



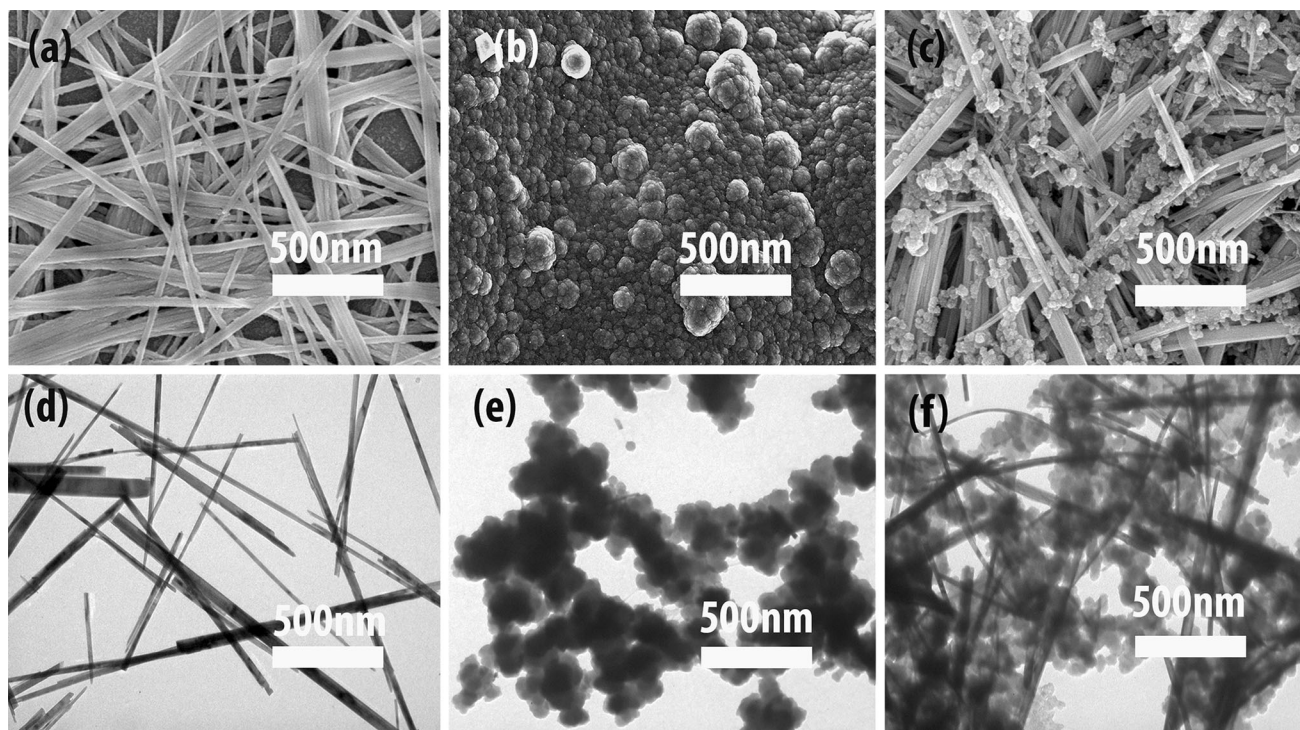


Fig. 1. Morphologies of (a, d) pristine  $\text{CeO}_2$ -NRs, (b, e) pure Ppy-NPs, and (c, f)  $\text{CeO}_2$ -NRs decorated with Ppy-NPs characterized by FE-SEM and TEM.

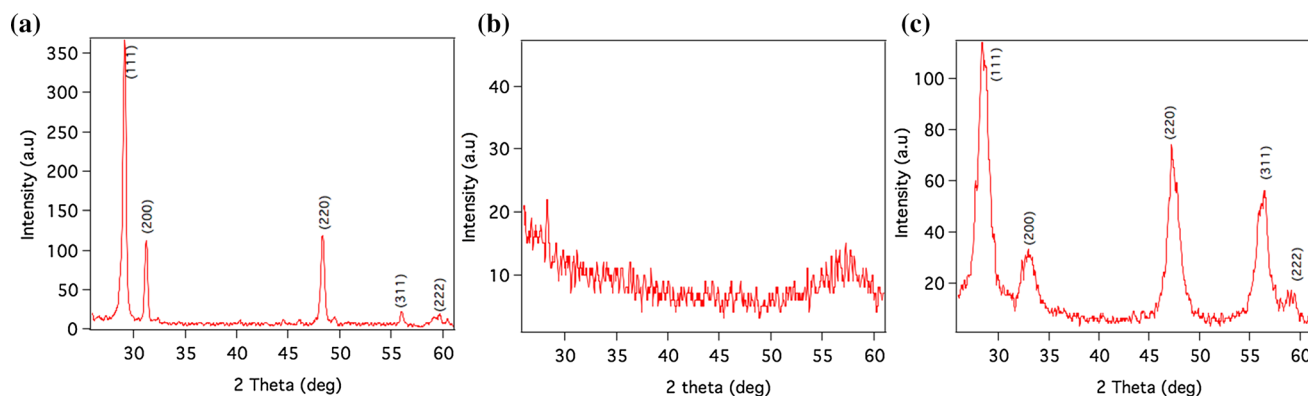


Fig. 2. X-ray diffraction patterns of (a) pristine  $\text{CeO}_2$ -NRs, (b) pure Ppy-NPs, and (c)  $\text{CeO}_2$ -NRs decorated with Ppy-NPs.

### DNA Hybridization Detection

An impedance analyzer (IM6) was used to determine the DNA hybridization. The output signal response was measured when dipping the modified electrode into 2 ml E-buffer solution containing 10 mM  $[\text{Fe}(\text{CN})_6]^{3-/4-}$  as an indicator probe. The prepared electrode was connected to the test and sense probes, and the Pt electrode was connected to the counterelectrode on the IM6 impedance analyzer with an Ag/AgCl reference electrode. All tests were conducted in open-circuit mode in the frequency range of 1 kHz to 100 kHz at amplitude of

$\pm 5$  mV. Bode plots were recorded, and differences in impedance modulus were considered as the signal to indicate DNA hybridization.

### Instrumentation

The morphology of the samples was explored by field-emission scanning electron microscopy (FE-SEM, JSM-7600F; JEOL) and transmission electron microscopy (TEM, JEM1010; JEOL). Infrared (IR) spectral characterization was performed on a Fourier-transform infrared (FTIR) spectrometer (NICOLET MEXUS 470; Thermo Electron Corporation).

X-ray diffraction (XRD) analysis was conducted on a D/Max 2500 V/PV x-ray diffractometer using Cu (40 kV, 30 mA) radiation. Photoluminescence spectra were recorded using a NANO LOG spectrofluorometer (Horiba, USA). An IM6 impedance analyzer was used for electrochemical measurements with a conventional three-electrode system and IM6-THALES software.

## RESULTS AND DISCUSSION

### Characteristics of CeO<sub>2</sub>-NRs, Ppy-NPs, and CeO<sub>2</sub>-NRs Decorated with Ppy-NPs

The morphologies of pristine CeO<sub>2</sub>-NRs, pure Ppy-NPs, and CeO<sub>2</sub>-NRs decorated with Ppy-NPs samples were investigated by FE-SEM and TEM (Fig. 1). FE-SEM and TEM images of pristine CeO<sub>2</sub>-NRs are shown in Fig. 1a and d, revealing uniform rod-like structure. Figure 1b and e show FE-SEM and TEM images of pure Ppy-NPs, revealing an aggregate cauliflower-like structure. FE-SEM and TEM images of CeO<sub>2</sub>-NRs decorated with Ppy-NPs

composites are shown in Fig. 1c and f, revealing that the Ppy-NPs were uniformly decorated on the CeO<sub>2</sub>-NRs.

The XRD patterns of (a) pristine CeO<sub>2</sub>-NRs, (b) pure Ppy-NPs, and (c) CeO<sub>2</sub>-NRs decorated with Ppy-NPs are shown in Fig. 2. The diffraction peaks at 28.6°, 33.1°, 47.6°, 56.5°, and 59.1° correspond to (111), (200), (220), (311), and (222) planes of the cubic fluorite structure of the pristine CeO<sub>2</sub>-NRs (Fig. 2a), indexed to Joint Committee on Powder Diffraction Standards (JCPDS) card no. 34-0394. Figure 2b shows the XRD pattern of the pure Ppy-NPs, indicating an amorphous structure due to the lack of defined peaks. The XRD pattern of CeO<sub>2</sub>-NRs decorated with Ppy-NPs is illustrated in Fig. 2c; The similar profile to that of pristine CeO<sub>2</sub>-NRs confirms that the crystal structure of CeO<sub>2</sub>-NRs was not modified by pure Ppy-NPs. However, when CeO<sub>2</sub>-NRs were decorated by Ppy-NPs, the intensity of the diffraction peaks decreased while their width increased compared with that of pristine CeO<sub>2</sub>-NRs. This result could be due to a decrease in crystallinity, assigned predominantly to the amorphous nature of Ppy, as reported in literature.<sup>24–26</sup>

Figure 3 shows the energy-dispersive x-ray spectroscopy results for the CeO<sub>2</sub>-NRs decorated with Ppy-NPs, where the appearance of Ce and O signals can be attributed to the CeO<sub>2</sub>-NRs. The appearance of the carbon signal confirms the presence of Ppy-NPs. No contaminating elements were detected in the CeO<sub>2</sub>-NRs decorated with Ppy-NPs during sample preparation, as indicated by the lack of peaks, except those for Si and Pt originating from the substrate.

### ssDNA Immobilization on Modified Electrode Surface

The density of ssDNA strands on the electrode modified with the CeO<sub>2</sub>-NRs decorated with Ppy-NP was studied by fluorescence microscopy. As shown in Fig. 4a, the surface of the modified electrode was

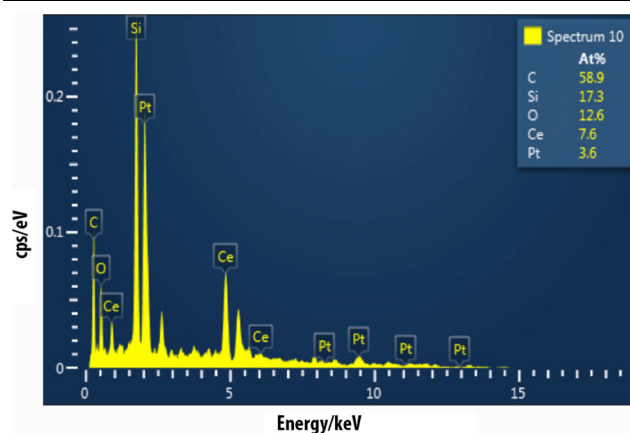


Fig. 3. Energy-dispersive x-ray analysis of CeO<sub>2</sub>-NRs decorated with Ppy-NPs.

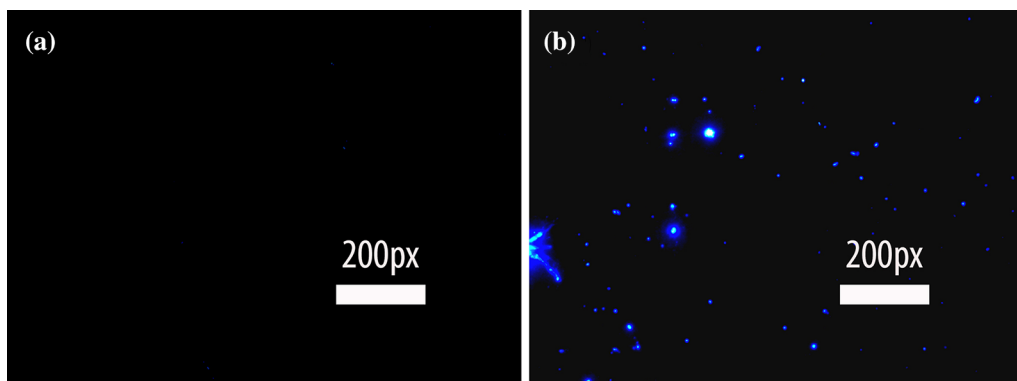


Fig. 4. Fluorescence images of (a) CeO<sub>2</sub>-NRs/Ppy-NPs modified electrode and (b) ssDNA/Ppy-NPs/CeO<sub>2</sub>-NRs electrode.

absolutely black while that with immobilized ssDNA showed white fluorescence spots (Fig. 4b). These results indicate successful immobilization of ssDNA sequences on the Ppy-NPs/CeO<sub>2</sub>-NR-modified electrode surface.

FTIR spectroscopy was performed to explore the molecular structure of the CeO<sub>2</sub>-NRs decorated with Ppy-NPs and the ssDNA sequences on the electrode surface. Figure 5a illustrates the FTIR spectra of the electrode modified with CeO<sub>2</sub>-NRs decorated with Ppy-NPs. The peaks at 3430 cm<sup>-1</sup> and 1540 cm<sup>-1</sup> are related to N–H and C–C stretching vibration in pyrrole ring.<sup>27</sup> A peak was also detected at 521 cm<sup>-1</sup>, corresponding to Ce–O stretching vibration of CeO<sub>2</sub>-NRs. The peak at 1385 cm<sup>-1</sup> is assigned to C–N stretching of pyrrole. The bands at 1299 cm<sup>-1</sup> are associated with C–N bonds. The band at 1028 cm<sup>-1</sup> is due to C–H deformation of pyrrole. The peak observed at 968 cm<sup>-1</sup> after the

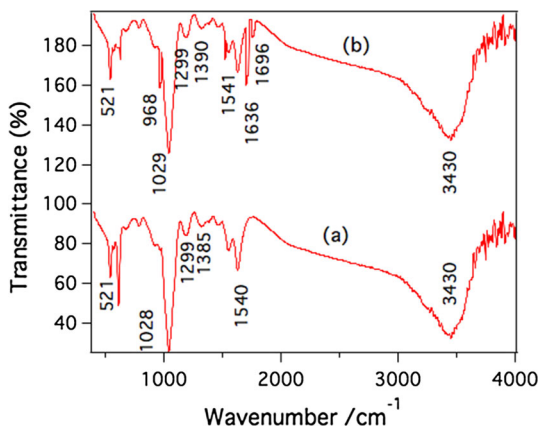


Fig. 5. FTIR spectra of (a) Ppy-NPs/CeO<sub>2</sub>-NRs electrode and (b) ssDNA-modified Ppy-NPs/CeO<sub>2</sub>-NRs electrode.

electrode surface was modified with ssDNA strands is related to the DNA backbone. The band at 1574 cm<sup>-1</sup> belongs to adenine (A). The vibration of the thymine (T) base in the DNA sequence was confirmed at 1663 cm<sup>-1</sup>. The absorption bands at ~ 521 cm<sup>-1</sup> are related to Ce–O stretching vibration of CeO<sub>2</sub>-NRs. The peaks at 1541 cm<sup>-1</sup> correspond to C–C stretching vibration of pyrrole ring. The vibrational mode of Ce–O–Ce was detected at 1390 cm<sup>-1</sup>. Additionally, the band of C–H deformation of Ppy shifted from 1028 cm<sup>-1</sup> to 1029 cm<sup>-1</sup>. The peak at 1690 cm<sup>-1</sup> is attributed to the GC base pair of the DNA sequence (Fig. 5b).

## Electrochemical Characterization of DNA Biosensor

### EIS Measurements

EIS measurements were carried out to obtain additional information on the DNA hybridization. The results are presented as Bode or phase plots, which express the logarithm of frequency versus the logarithm of the impedance modulus or phase angle. Figure 6A presents the Bode plots of the DNA sensor after hybridization with complementary DNA. As shown in Fig. 6A, the frequency range from 10 kHz to 100 kHz illustrates ionic conduction between the electrode and electrolyte ( $R_s$ ). The frequency range from 1 kHz to 10 kHz is related to the double-layer capacitance ( $C_{dl}$ ), while the range from 1 Hz to 1 kHz is associated with the charge-transfer resistance ( $R_{ct}$ ). The Bode plot of the bare electrode in buffer solution containing the redox probe 5 mM [Fe(CN)<sub>6</sub>]<sup>3-/4-</sup> is indicated in Fig. 6A(a). After modification of the electrode surface by CeO<sub>2</sub>-NRs [Fig. 6A(b)], the layer of CeO<sub>2</sub>-NRs can hinder electron transfer from the redox probe [Fe(CN)<sub>6</sub>]<sup>3-/4-</sup> to the electrode surface, thereby increasing the impedance modulus. When

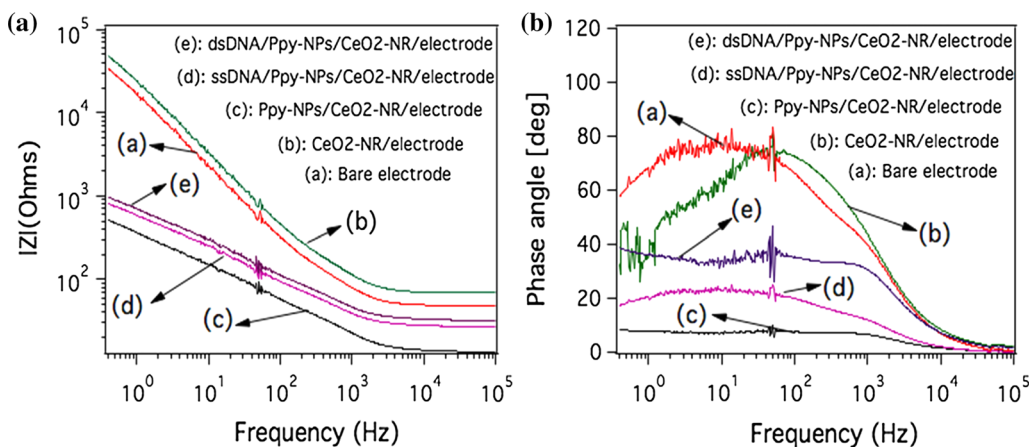


Fig. 6. (A) Bode plots of impedance modulus and (B) phase angle recorded for (a) bare electrode, (b) CeO<sub>2</sub>-NRs/electrode, (c) Ppy-NPs/CeO<sub>2</sub>-NRs electrode, (d) ssDNA/Ppy-NPs/CeO<sub>2</sub>-NRs electrode, and (e) dsDNA/Ppy-NPs/CeO<sub>2</sub>-NRs electrode.



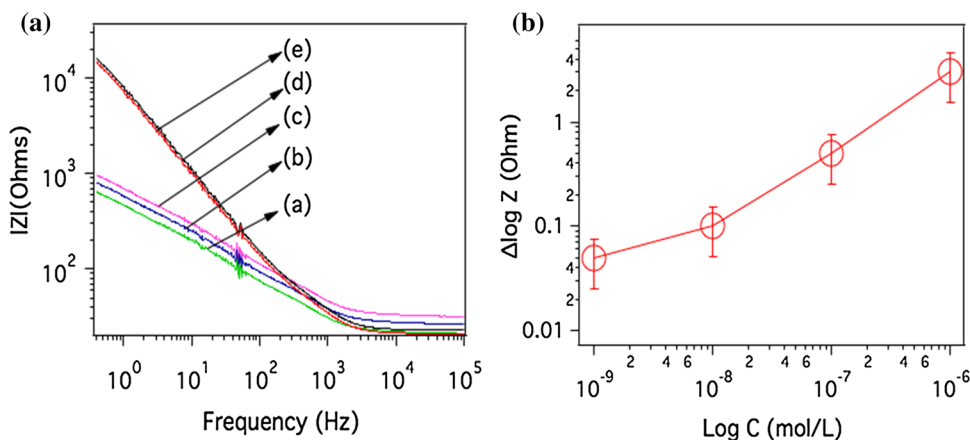


Fig. 7. (A) Bode plots recorded (a) at the ssDNA/Ppy-NPs/CeO<sub>2</sub>-NRs electrode, and after hybridization with different concentrations (b)  $1.0 \times 10^{-9}$  mol L<sup>-1</sup>, (c)  $1.0 \times 10^{-8}$  mol L<sup>-1</sup>, (d)  $1.0 \times 10^{-7}$  mol L<sup>-1</sup>, and (e)  $1.0 \times 10^{-6}$  mol L<sup>-1</sup>. (B) Plot of  $\Delta \log Z$  versus the logarithm of the target DNA concentration.

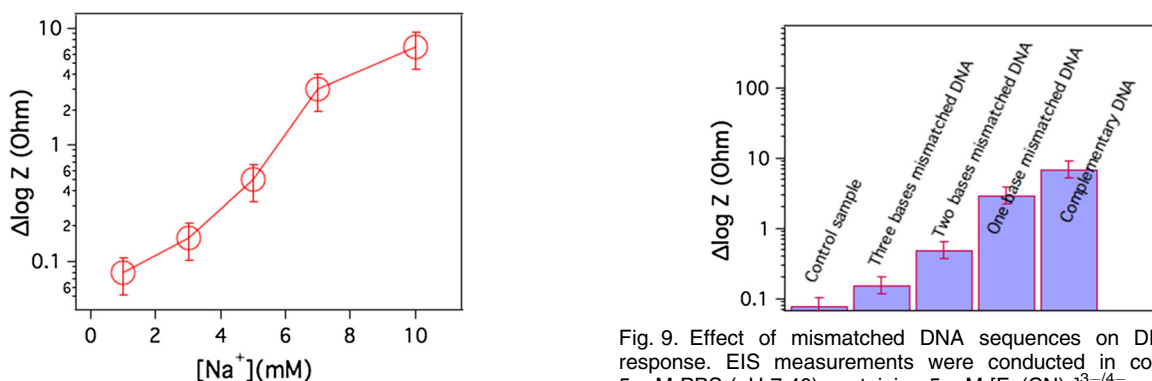


Fig. 8. Effect of Na<sup>+</sup> ionic strength in the hybridization buffer on DNA detection. The concentration is  $1.0 \times 10^{-6}$  mol L<sup>-1</sup>. EIS measurements were conducted in conditions of 5 mM PBS (pH 7.40) containing 5 mM [Fe(CN)<sub>6</sub>]<sup>3-/4-</sup>.

the electrode surface was modified by CeO<sub>2</sub>-NRs decorated with Ppy-NPs, the impedance modulus decreased. This low value of the impedance modulus may be due to the more electroactive electrode surface caused by CeO<sub>2</sub>-NRs decorated with Ppy-NPs, thereby facilitating electron transfer between the electrolyte medium and electrode within the range of 1 Hz to 100 kHz [Fig. 6A(c)]. After modification of the electrode surface by the ssDNA sequences (ssDNA/Ppy-NPs/CeO<sub>2</sub>-NRs electrode), the absolute impedance increased, indicating that [Fe(CN)<sub>6</sub>]<sup>3-/4-</sup> was prevented from reaching the electrode surface due to limitation by the negatively charged phosphate backbone of the ssDNA<sup>28</sup> [Fig. 6-A(d)]. The impedance modulus increased further after DNA hybridization. The formation of this duplex increased the negative charge on the electrode surface, blocking access by the redox probe

[Fe(CN)<sub>6</sub>]<sup>3-/4-</sup> [Fig. 6A(e)]. The signal was unchanged when the ssDNA/Ppy-NPs/CeO<sub>2</sub>-NRs electrode was exposed to the control sample (data not shown). The change in the phase plots is indicated in Fig. 6(B). Phase angles of 77°, 75°, 9°, 19°, and 37° were obtained for the bare sensor, CeO<sub>2</sub>-NRs electrode, Ppy-NPs/CeO<sub>2</sub>-NRs electrode, ssDNA/Ppy-NPs/CeO<sub>2</sub>-NRs electrode, and dsDNA/Ppy-NPs/CeO<sub>2</sub>-NRs electrode, respectively. The phase angle changed to 9° when the electrode was modified by CeO<sub>2</sub>-NRs decorated with Ppy-NPs due to the enhanced electron transfer rate. The phase angle changed again to 19° when ssDNA was immobilized on the modified electrode, because the negatively charged ssDNA was attached to the electrode covalently, thereby preventing [Fe(CN)<sub>6</sub>]<sup>3-/4-</sup> from reaching the electrode surface. After hybridization with the dsDNA sequence, the phase angle increased due to duplex formation; consequently, [Fe(CN)<sub>6</sub>]<sup>3-/4-</sup> had more difficulty in approaching the electrode surface through the

Fig. 9. Effect of mismatched DNA sequences on DNA sensor response. EIS measurements were conducted in conditions of 5 mM PBS (pH 7.40) containing 5 mM [Fe(CN)<sub>6</sub>]<sup>3-/4-</sup>.

channels of the double-stranded DNA (dsDNA) duplex.

#### Effect of Complementary Sequence Concentration

The effect of the target DNA sequence was explored at different concentrations (Fig. 7A, B). The difference between the  $\log(Z)$  value of the ssDNA/Ppy-NPs/CeO<sub>2</sub>-NRs electrode and that after hybridization was considered as the measurement signal. After hybridization with the target DNA, the impedance increased within the range from  $1.0 \times 10^{-9}$  mol L<sup>-1</sup> to  $1.0 \times 10^{-6}$  mol L<sup>-1</sup> with a regression equation of  $\Delta \log Z = 2.94 \times 10^6 \log C + 0.1059$  and regression coefficient ( $R$ ) of 0.999, where  $C$  is the concentration of the target DNA sequence. The sensitivity of the DNA sensor was estimated as  $14.7 \times 10^6 \Omega/\text{mol L}^{-1} \text{ cm}^{-2}$ . The limit of detection (LOD) and limit of quantification (LOQ) of the DNA biosensor were calculated using the equations  $\text{LOD} = 3S_b/S$  and  $\text{LOQ} = 10S_b/S$ ,<sup>29</sup> respectively, where  $S_b$  is the standard deviation of the blank signal and  $S$  is the sensitivity. The LOD and LOQ of the fabricated DNA biosensor were  $2.86 \cdot 10^{-7}$  mol L<sup>-1</sup> and  $9.56 \cdot 10^{-7}$  mol L<sup>-1</sup>, respectively.

#### Effect of Ionic Strength on DNA Sensor Response

As mentioned in Ref. 30, observation of hybridization without NaCl in the hybridization buffer is difficult. Therefore, the DNA hybridization was studied at different NaCl concentrations (Fig. 8). The response of the DNA sensor gradually increased with increasing NaCl concentration from 1 mM to 10 mM because of the reduced electric repulsion among the DNA nucleotides, leading to an increased binding rate between the DNA probe and its complementary.<sup>31</sup> The melting temperature of the dsDNA ( $T_m$ ) influences the DNA hybridization. As  $T_m$  increases, the hybridization rate also gradually increases.<sup>32</sup> According to Surzycki et al.,<sup>33</sup>  $T_m$  can be calculated as

$$T_m = 81.5 + 0.04(\%GC) + 16.6 \log[M^+], \quad (1)$$

where  $M^+$  is the molar concentration of the monovalent cation Na<sup>+</sup>. According to Eq. 1, when the Na<sup>+</sup> concentration increases, so does  $T_m$ . Consequently, the hybridization rate increases, thereby improving the response of the DNA sensor.

#### Effect of Mismatched DNA Sequences on Output Signal Response of DNA Sensor

Figure 9 shows the  $\Delta \log(Z)$  value of the DNA sensor hybridized with the control sample, one-base-mismatched DNA, two-base-mismatched DNA, three-base-mismatched DNA, and the full complementary in PBS solution. The  $\Delta \log(Z)$  value for hybridization with the full complementary was the highest compared with the base-mismatched DNA sequences. As the number of mismatched bases

increased, the  $\Delta \log(Z)$  value decreased. The hybridization efficiency decreased because the mismatched DNA sequence negatively affected the formation of some double helices.

#### Stability, Regeneration, and Reproducibility of DNA Biosensor

Stability is one of the factors that influence the performance of DNA sensors. In this work, the stability of the DNA biosensor was evaluated. The ssDNA/Ppy-NPs/CeO<sub>2</sub>-NRs electrode was stored in a refrigerator at 4°C for 3 months after evaluation via EIS measurements. No apparent change in the EIS signals was observed after 3 weeks. However, the output signal response of the DNA sensor had decreased by approximately 32% after 8 weeks. The signal response was undetectable when the DNA biosensor was stored in PBS (pH 7.0) at 4°C for 12 weeks because of the decreased biological activity of the DNA probe, which no longer bound to its complementary. These results confirm the favorable stability of the developed DNA biosensor.

Reusability is another factor that plays an important role in continuous monitoring of target DNA. In this work, the DNA sensor was regenerated by dipping the dsDNA/CeO<sub>2</sub>-NR@Ppy electrode in hot water at 98°C for 5 min then quickly freezing in an ice bath for 2 min to obtain ssDNA/CeO<sub>2</sub>-NR@Ppy electrode. The developed DNA sensor could be regenerated two to three times with about 15% to 17% loss of the original signal. The signal attenuation could be due to denaturation of the DNA sequences on the surface of the sensor. The renewed DNA biosensor could be used again for target DNA detection.

To evaluate the reproducibility of the DNA biosensor, ten DNA biosensors were prepared to detect the target DNA sequence at concentration of  $1.0 \times 10^{-6}$  mol L<sup>-1</sup>. The results showed that the relative standard deviation of the signal change measured by the ten biosensors was 3.01%, indicating acceptable reproducibility for DNA analysis.

## CONCLUSIONS

A simple, selective, and high-sensitivity DNA sensor was successfully developed by using CeO<sub>2</sub>-NRs decorated with Ppy-NPs for label-free detection of *Salmonella*. The as-prepared nanocomposite offers numerous excellent sites for ssDNA sequence immobilization on the electrode surface with increased electron transfer rate. The modified electrode was characterized using different approaches such as FE-SEM, XRD, and FTIR analyses. The output signal response of the DNA biosensor was explored by EIS measurements with [Fe(CN)<sub>6</sub>]<sup>3-/4-</sup> as an electrochemical probe. The developed DNA sensor showed good linearity from  $1.0 \times 10^{-9}$  mol L<sup>-1</sup> to  $1.0 \times 10^{-6}$  mol L<sup>-1</sup> and sensitivity of  $14.7 \times 10^6 \Omega/\text{mol L}^{-1} \text{ cm}^{-2}$ . The DNA biosensor showed an LOD of  $2.86 \times 10^{-7}$  mol L<sup>-1</sup>



and an LOQ of  $9.56 \times 10^{-7}$  mol L<sup>-1</sup>. In future work, the developed sensor could be used to detect not only *Salmonella* in real samples but also other pathogens.

### ACKNOWLEDGMENTS

This work was funded by the Vietnam National Foundation for Science and Technology Development (Grant No. 103.02-2015.50).

### REFERENCES

1. H. Li, U.B. Gyllensten, X. Cui, R.K. Saiki, H.A. Erlich, and N. Arnheim, *Nature* 335, 414 (1988).
2. Y.Q. Du, P.F. Gao, W. Wang, T.T. Wang, Y. Chang, J. Wang, and ChZh Huang, *Analyst* 138, 5745 (2013).
3. R.P. Stokes, A. Cordwell, and R.A. Thompson, *J. Clin. Pathol.* 35, 566 (1982).
4. C.S. Riccardi, H. Yamanaka, M. Josowicz, J. Kowalik, B. Mizaikoff, and C. Kranz, *Anal. Chem.* 78, 1139 (2006).
5. Y. Guo, J.H. Chen, and C. Guonan, *Sens. Actuator B-Chem.* 184, 113 (2013).
6. C. Singhal, M. Khanuja, N. Chaudhary, C.S. Pundir, and J. Narang, *Sci. Rep.* 8, 7734 (2018).
7. Z. Liu and X. Su, *Biosens. Bioelectron.* 87, 66 (2017).
8. M. Mehrgardi and L. Ahangar, *Biosens. Bioelectron.* 26, 4308 (2011).
9. C.P.S. Liew, B. Lertanantawong, S.Y. Lee, R. Manickam, Y.H. Lee, and W.S. Chai, *Talanta* 139, 167 (2015).
10. G. Martínez-Paredes, M.B. González-García, and A. Costa-García, *Sens. Actuator B-Chem.* 149, 329 (2010).
11. A.C. Lee, D. Du, B. Chen, C.K. Heng, T.M. Lim, and Y. Lin, *Analyst* 139, 4223 (2014).
12. M. Asghary, J.B. Raoof, M. Rahimnejad, and R. Ojani, *Biosens. Bioelectron.* 82, 173 (2016).
13. A. Liu, K. Wang, S. Weng, Y. Lei, K. Lin, W. Chen, X. Lin, and Y. Chen, *Trends Anal. Chem.* 37, 101 (2012).
14. M. Mohammed, I.J. Ibraheem, A.S. Obaid, and M. Bououdina, *Sens. Biosensing Res.* 15, 46 (2017).
15. P.A. Rasheed and N. Sandhyarani, *Biosens. Bioelectron.* 15, 226 (2017).
16. S. Peschel, B. Ceyhan, C.M. Niemeyer, S. Gao, L. Chi, and U. Simon, *Mater. Sci. Eng., C* 19, 47 (2002).
17. W. Gao, X. Wei, X. Wang, G. Cui, Z. Liua, and B. Tang, *Chem. Commun.* 52, 3643 (2016).
18. N.T. Nguyet, L.T.H. Yen, V.V. Thu, H. Lan, T. Trung, P.H. Vuong, and P.D. Tam, *J. Phys. Chem. Solids* 115, 18 (2018).
19. M.B. Gumpu, N. Nesakumar, S. Sethuraman, U.M. Krishnan, and J.B.B. Rayappan, *Sens. Actuators B –Chem.* 199, 330 (2014).
20. M. Singh, N. Nesakumar, S. Sethuraman, U.M. Krishnan, and J.B.B. Rayappan, *J. Colloid Interface Sci.* 425, 52 (2014).
21. Q. Wang, F. Gao, X. Zhang, B. Zhang, S. Li, Z. Hu, and F. Gao, *Electrochim. Acta* 62, 250 (2012).
22. W. Zhang, T. Yang, X. Zhuang, Z. Guo, and K. Jiao, *Biosens. Bioelectron.* 24, 2417 (2009).
23. X. Qian, Q. Qu, L. Li, X. Ran, L. Zuo, R. Huang, and Q. Wang, *Sensors* 18, 1878 (2018).
24. U. Baig, M.A. Gondal, A.M. Ilyas, and M.M. Sanagi, *J. Mater. Sci. Technol.* 33, 547 (2017).
25. S. Peshoria and A.K. Narula, *J. Mater. Sci.* 53, 3876 (2018).
26. M. Bruck, C.N. Gannett, D.C. Bock, P.F. Smith, A.C. Marschilok, K.J. Takeuchi, and E.S. Takeuchi, *J. Electrochem. Soc.* 164, A6260 (2017).
27. J. Zhang and X.S. Zhao, *J. Phys. Chem. C* 116, 5420 (2012).
28. F. Li, X. Han, and S. Liu, *Biosens. Bioelectron.* 26, 2619 (2011).
29. M. Singh, N. Nesakumar, S. Sethuraman, U.M. Krishnan, and J.B.B. Rayappan, *J. Colloid Interface Sci.* 425, 52 (2014).
30. X.C. Zhou, L.Q. Huang, and S.F.Y. Li, *Biosens. Bioelectron.* 16, 85 (2001).
31. Y. Okahata, M. Kawase, K. Niilura, F. Ohtake, H. Furusawa, and Y. Ebara, *Anal. Chem.* 70, 1288 (1998).
32. P.D. Tam, M.A. Tuan, N.V. Hieu, and N.D. Chien, *Physica E* 41, 1567 (2009).
33. S. Surzycki, *Human Molecular Biology Laboratory Manual* (Wiley - Blackwell, 2003), ISBN 9780632046768..

**Publisher's Note** Springer Nature remains neutral with regard to jurisdictional claims in published maps and institutional affiliations.